Supporting Information

Hydrogen-bonded organic framework with tailored pores prepared by enlarging the core size for high-performance Xe/Kr separation

*Zhen Yuan, Liangji Chen, Xin Zhou, Lu Li, Yunbin Li, Yisi Yang, Zhiqi Zhou, Yanting Chen, Shengchang Xiang, Banglin Chen, Zhangjing Zhang**

Fujian Key Laboratory of Polymer Materials, College of Chemistry and Materials Science, Fujian Normal University, 32 Shangsan Road, Fuzhou 350007

*Corresponding Authors: zzhang@fjnu.edu.cn

Table of contents

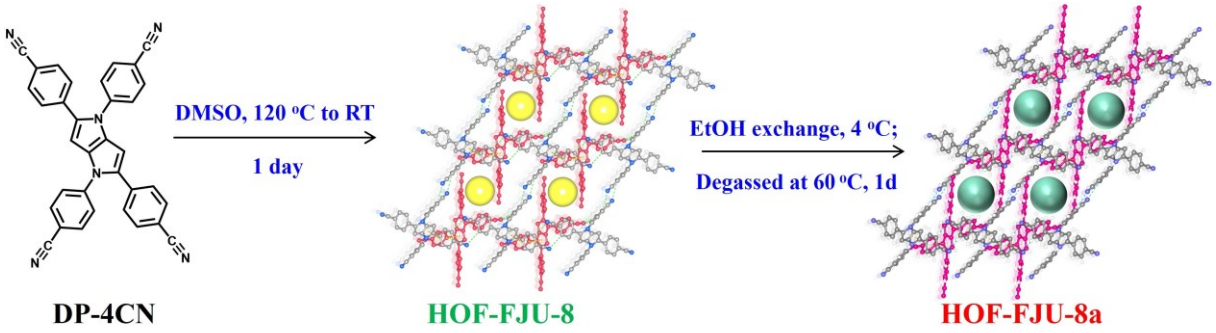

Scheme S1. Synthesis procedure for HOF-FJU-8a.

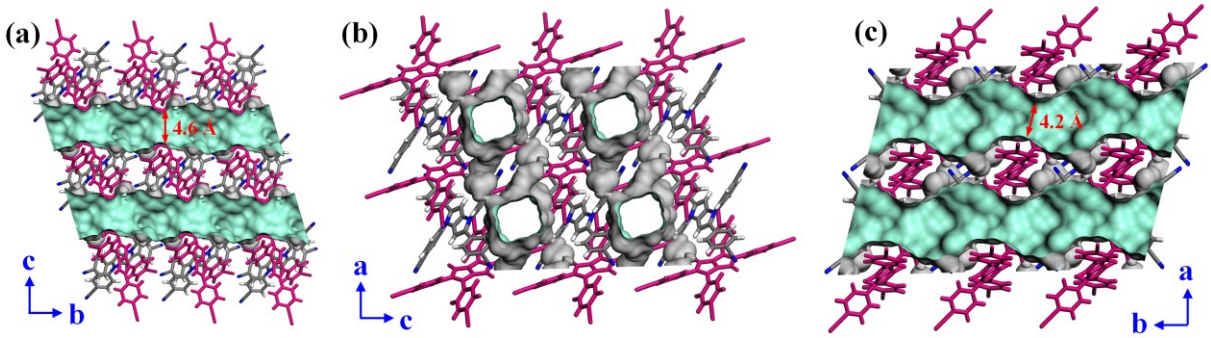

Figure S1. Stacking diagram of HOF-FJU-8a with different crystal axial directions: (a) *a* axis; (b) *b* axis; (c) *c* axis. Indicating the 1D open channels along *b* axis.

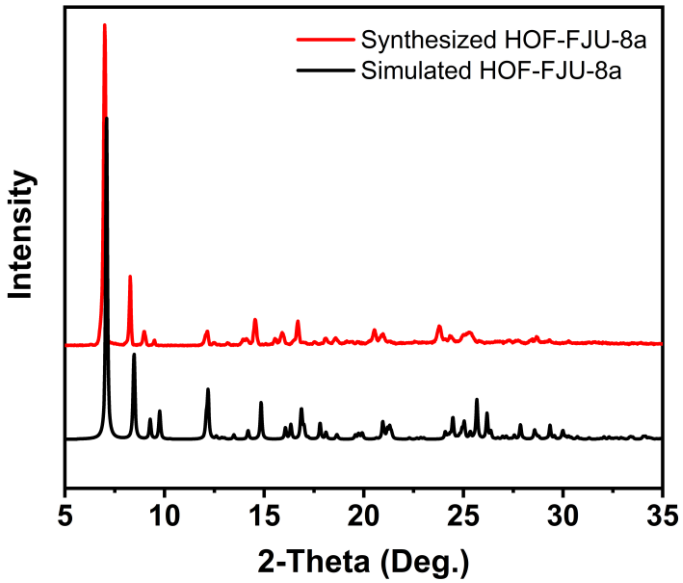

Figure S2. The powder X-ray diffraction patterns of HOF-FJU-8a for the simulated and as synthesized.

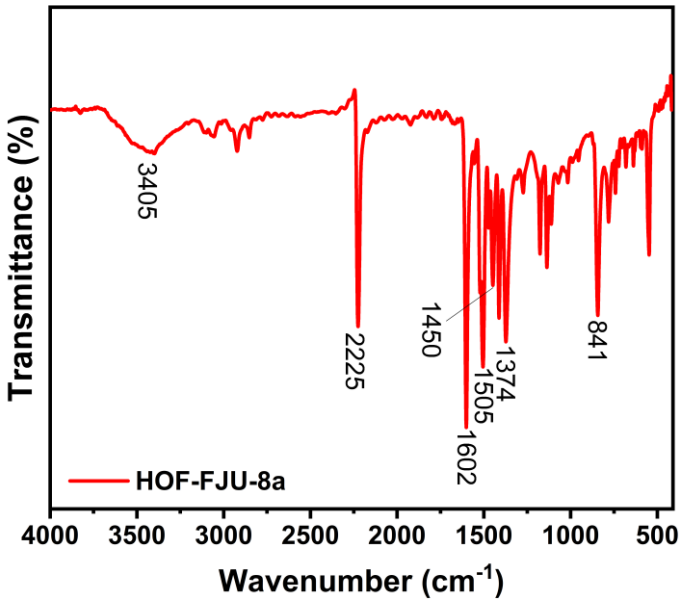

Figure S3. FTIR spectra of HOF-FJU-8a. The peak at 3405 cm^{-1} corresponds to the N-H bond stretching vibration in the dipyrrole moiety, the peak at 1450 cm^{-1} is attributed to the C-N bond stretching vibration in the dipyrrole. The presence of a cyano group is confirmed by the peak at 2225 cm^{-1}. Peaks at 1602 and 1505 cm^{-1} are indicative of C=C bonds. Bending vibrations of C-H bonds from aromatic rings are observed at 1374 and 841 cm^{-1}. This analysis underscores the chemical structural characteristics of HOF-FJU-8a are consistence with its monomer, DP-4CN.

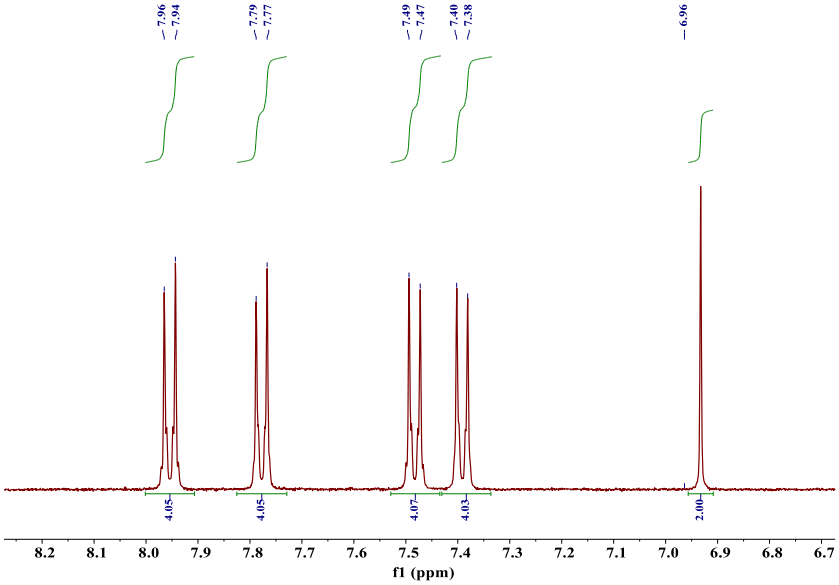

Figure S4. ^{1}H-NMR spectra of HOF-FJU-8a in DMSO-d6. The result indicates that the chemical structure of HOF-FJU-8a is consistent with its monomer molecular DP-4CN.

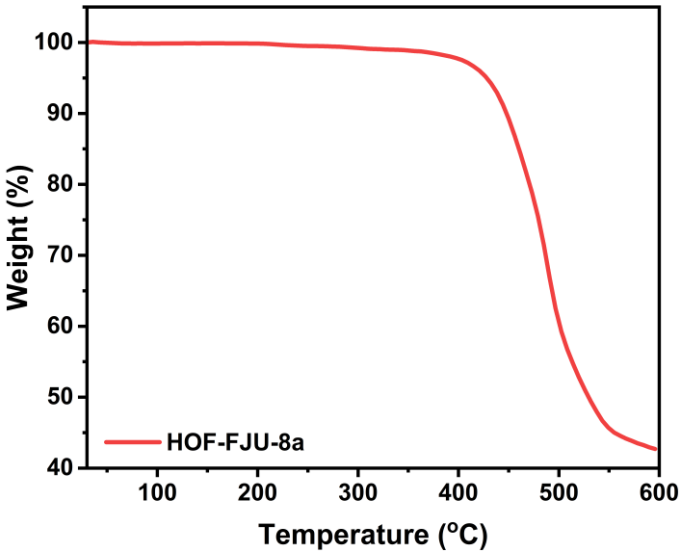

Figure S5. The TGA curve of HOF-FJU-8a under N_2 atmosphere.

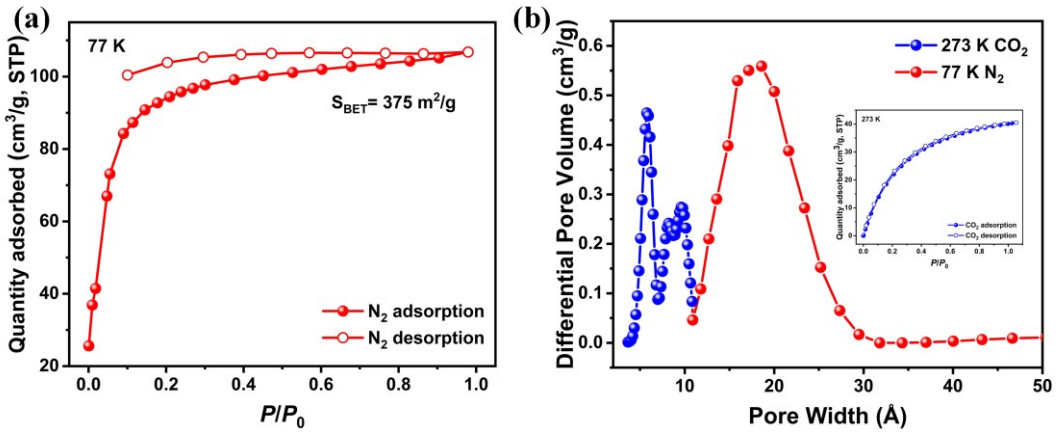

Figure S6. (a) N_2 adsorption isotherm of HOF-FJU-8a at 77 K. (b) The pore size distribution of HOF-FJU-8a derived from N_2 adsorption isotherm at 77 K and CO_2 adsorption isotherm at 273 K.

The isosteric enthalpies of adsorption (Q_{st}) calculation

The isosteric enthalpy of adsorption for Xe and Kr were calculated using the data collected at 273 K and 296 K. The data were fitted first using a virial-type expression composed of parameters a_i and b_i (eq 1). Then, the Q_{st} (kJ mol^{-1}) was calculated from the fitting parameters using eq 2, where p is the pressure (mmHg), T is the temperature (K), R is the universal gas constant (8.314 J·mol^{-1}·K^{-1}), N is the amount adsorbed (mg g^{-1}), and m and n determine the number of terms required to adequately describe the isotherm.

$$In\ p = In\ N + \frac{1}{T}\sum_{i=0}^{m} a_i\, n^i + \sum_{i=0}^{n} b_i n^i \qquad (1)$$

$$Q_{st} = -\,R\sum_{i=0}^{m} a_i n^i \qquad (2)$$

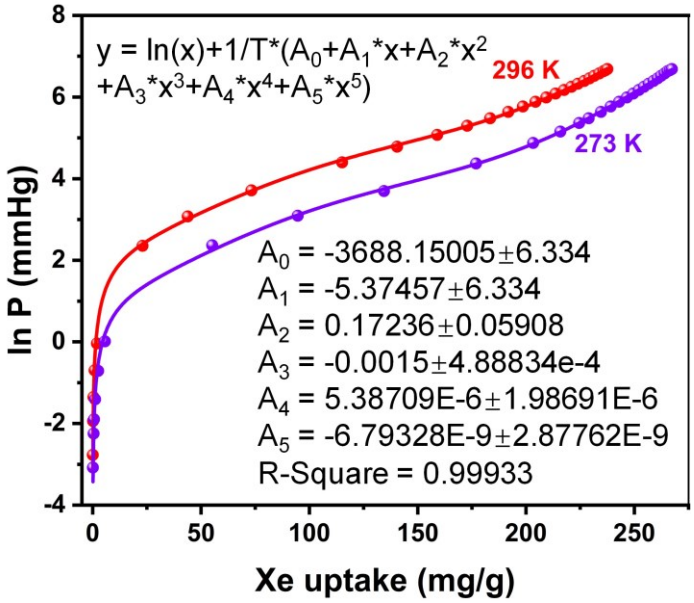

Figure S7. Experimental data (sphere) and fitting curve (solid line) of Xe adsorption isotherms of HOF-FJU-8a at 273 and 296 K, based on the virial-type expression.

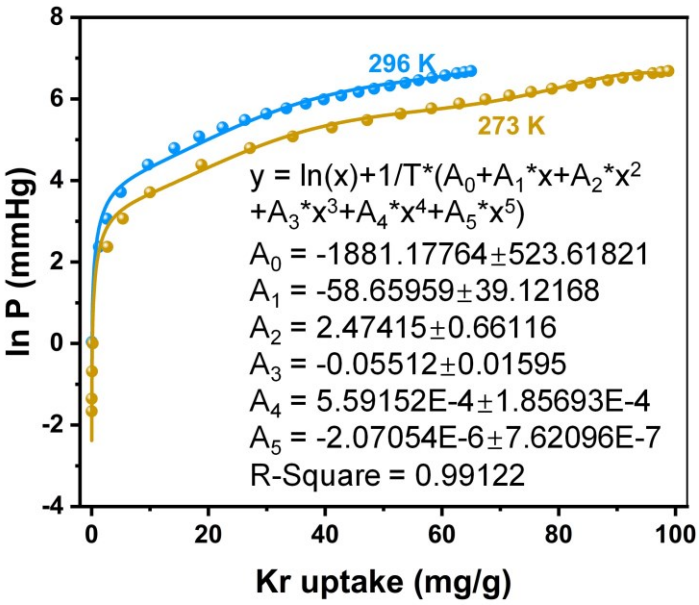

Figure S8. Experimental data (sphere) and fitting curve (solid line) of Kr adsorption isotherms of HOF-FJU-8a at 273 and 296 K, based on the virial-type expression.

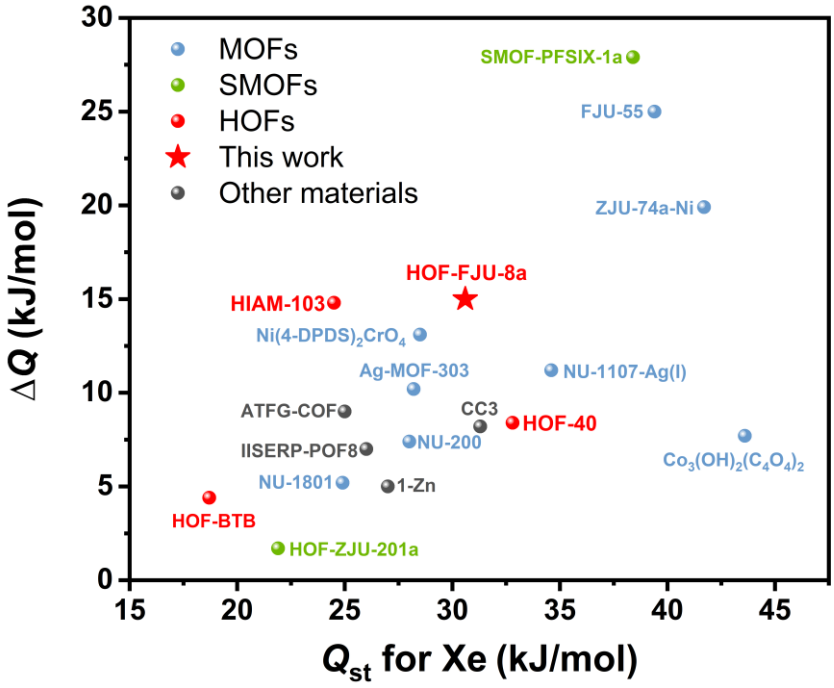

Figure S9. Comparison of the Q_{st} (Xe) and ΔQ_{st} of HOF-FJU-8a with some representative porous materials.

Prediction of the gas adsorption selectivity by IAST

Fitting details: the adsorption data for Xe and Kr in HOF-FJU-8a at 273 and 296 K were fitted with single-site Langmuir-Freundlich equation.

$$N = N^{\max} \times N\frac{\mathrm{b}p^{1/n}}{1+bp^{1/n}} \qquad (3)$$

where p is the pressure of the bulk gas in equilibrium with the adsorbed phase (kPa), N is the amount adsorbed per mass of adsorbent (mmol g^{-1}), $N^{\max}$ is the saturation capacities of site 1 (mmol g^{-1}), b is the affinity coefficients of site 1 (1/kPa) and n represents the deviations from an ideal homogeneous surface.

IAST calculation[1]: The adsorption selectivity based on IAST for Xe/Kr mixed is defined by the following equation:

$$S_{A/B} = \frac{q_A y_B}{q_B y_A} \qquad (4)$$

where q_i and y_i are the mole fractions of component i (i = A, B) in the adsorbed and bulk phases, respectively.

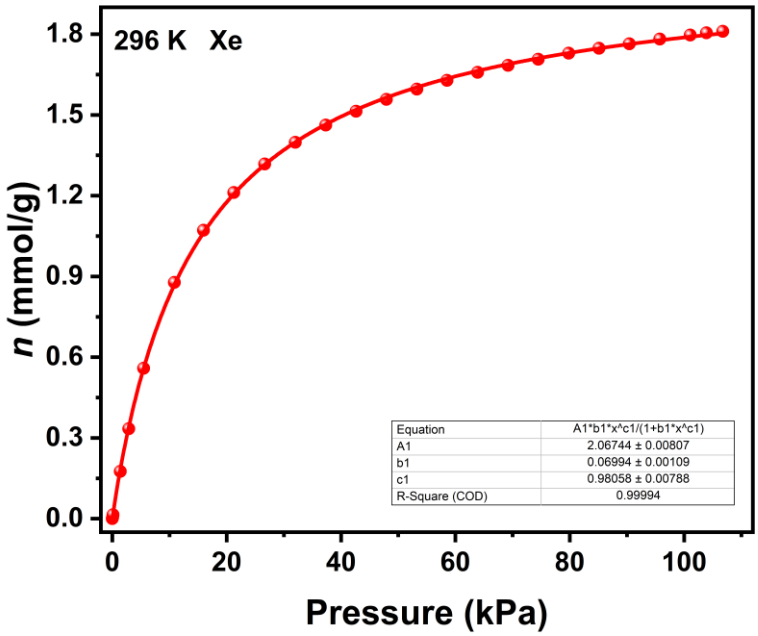

Figure S10. Single-site Langmuir-Freundlich equations fit for adsorption of Xe on HOF-FJU-8a at 296 K.

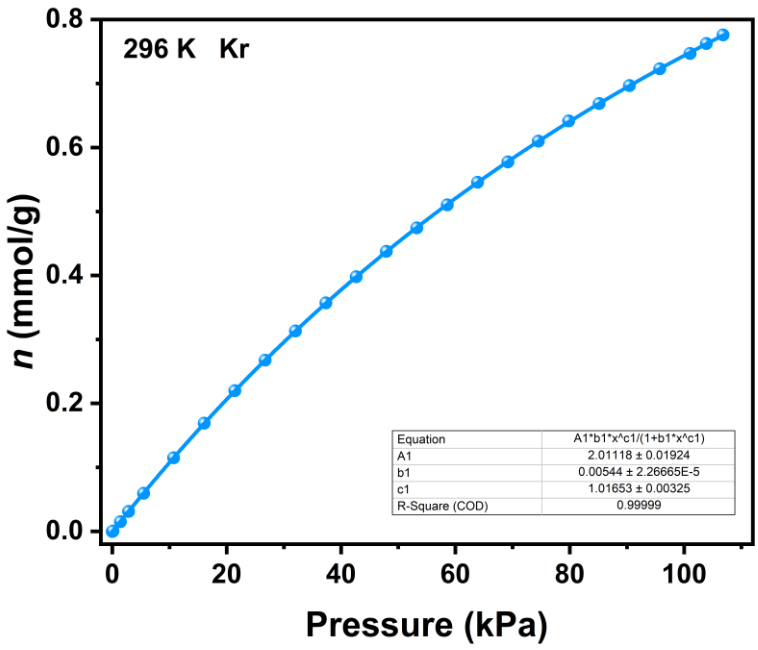

Figure S11. Single-site Langmuir-Freundlich equations fit for adsorption of Kr on HOF-FJU-8a at 296 K.

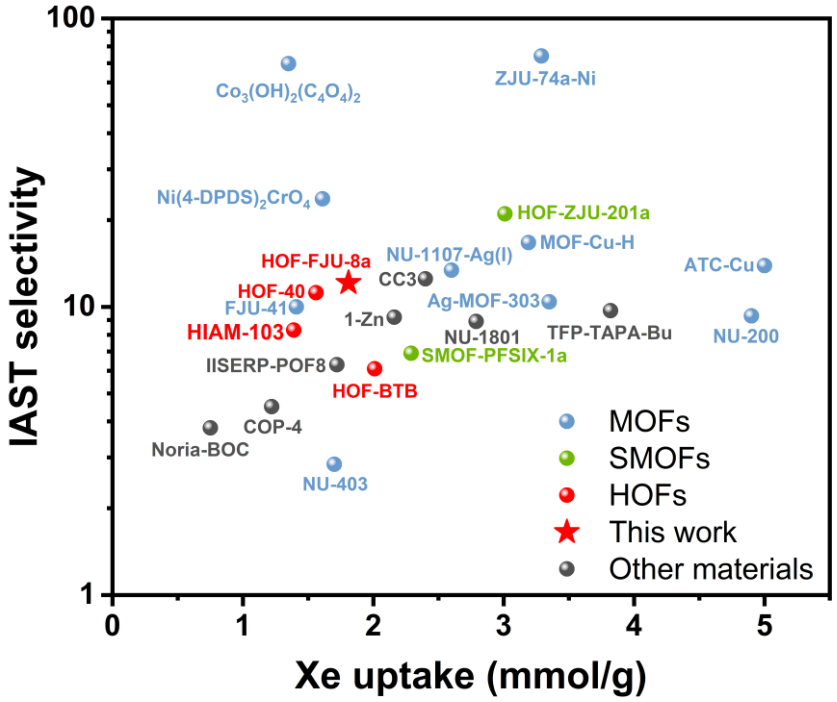

Figure S12. Comparison of the Xe uptake and IAST selectivity of HOF-FJU-8a with some representative porous materials.

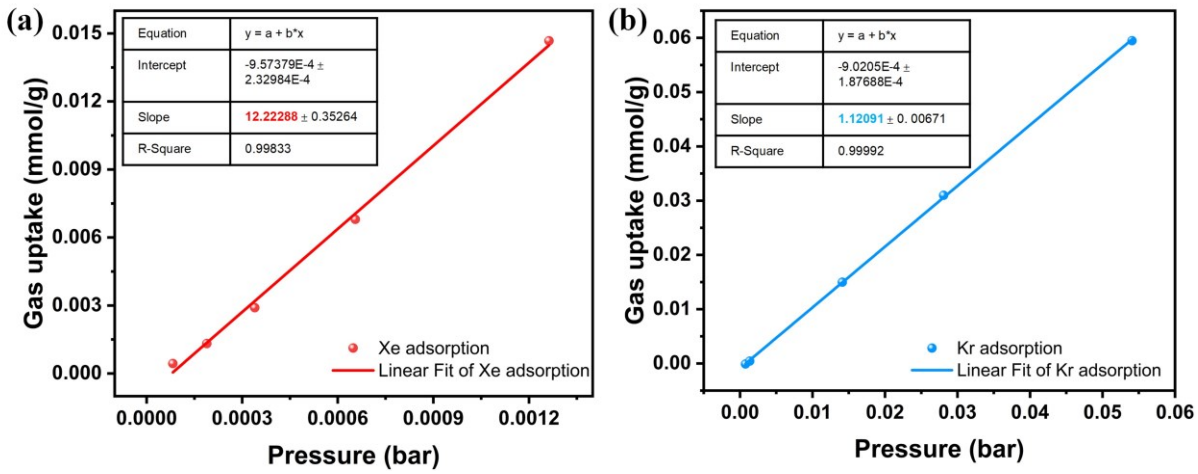

Figure S13. Henry coefficient fitting of Xe (a) and Kr (b) adsorption isotherms of HOF-FJU-8a at 296 K. Henry's constant is a useful measure of the adsorbent affinity for adsorbates since it represents the partition of the adsorbate between its bulk phase and adsorbed phase at very low pressures.

Henry′s Constant of HOF-FJU-8a (296 K) = $H_{Xe} \div H_{Kr}$ = 12.22288 ÷ 1.12091 = 10.9

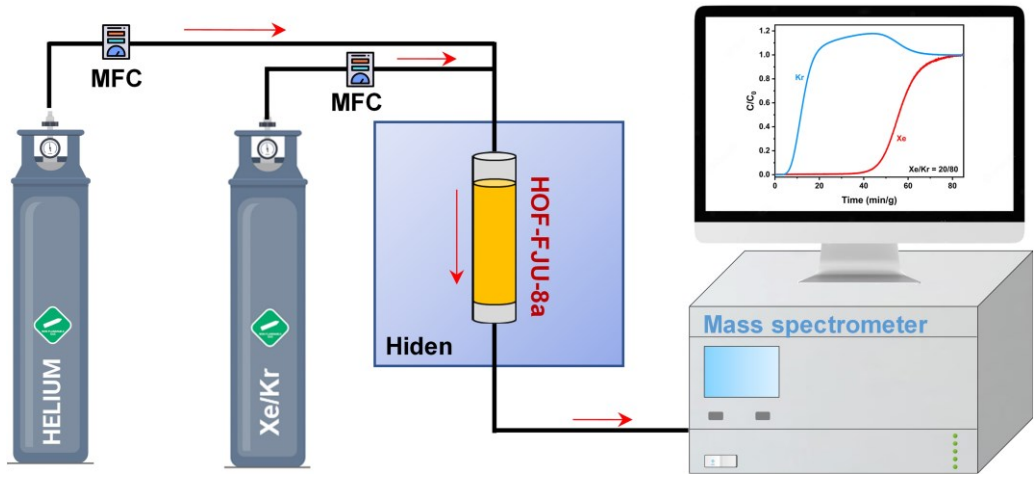

Figure S14. Schematic illustration of the apparatus for the breakthrough experiments.

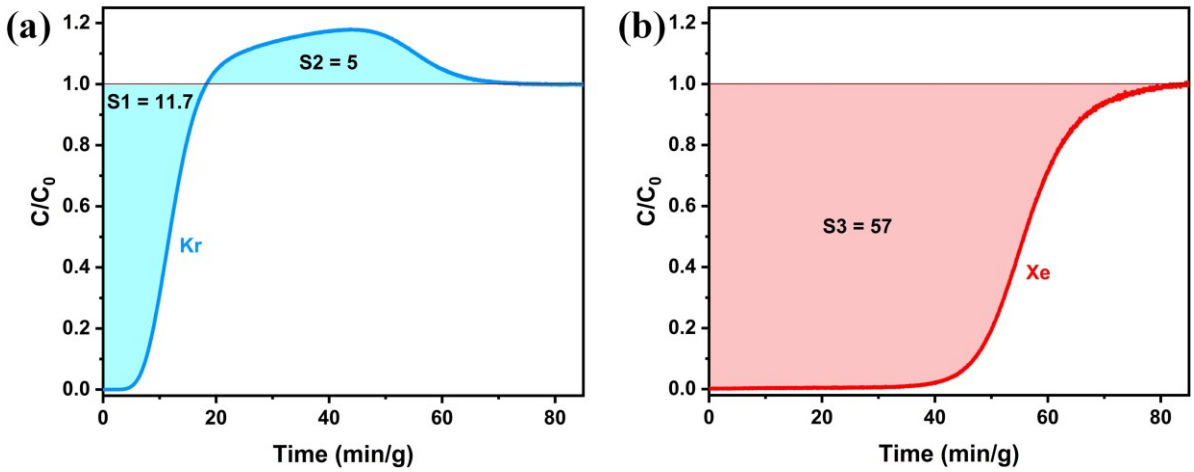

Figure S15. The calculation for the captured amount of Kr and Xe during the breakthrough process in HOF-FJU-8a.

The dynamic uptake capacities of Xe (q_{Xe}) and Kr (q_{kr}) were calculated as:

$$q_{Xe} = v \times y_{Xe} \times S_{Xe} \div 22.4 = 2 \times 0.2 \times 57 \div 22.4 = 1.02 \text{ mmol/g};$$

$$q_{kr} = v \times y_{Kr} \times S_{Kr} \div 22.4 = 2 \times 0.8 \times (11.7\text{-}5.66) \div 22.4 = 0.48 \text{ mmol/g};$$

The separation factor (α) was calculated as:

$$\alpha_{Xe/Kr} = (q_{Xe}/q_{kr}) \div (y_{Xe}/y_{kr}) = (1.02/0.48) \div (0.2/0.8) = 8.50$$

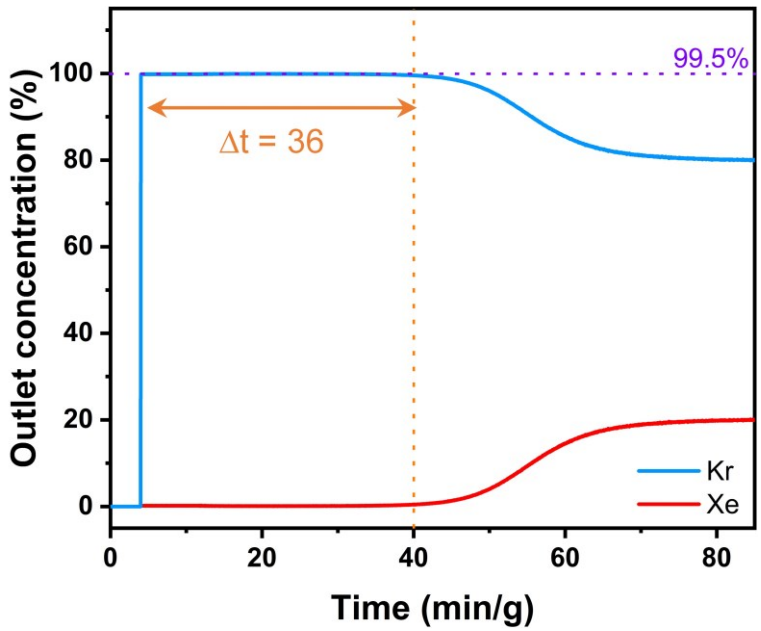

Figure S16. Experimental column breakthrough curves for the mixture of Xe/Kr (20/80) with HOF-FJU-8a at 296 K at a total flow of 2.0 mL/min.

The dynamic breakthrough productivity of Kr (Q_{Kr}) was calculated as:

$$Q_{Kr} = \Delta t \times v = 36 \times 2 = 72 \text{ L/kg}$$

The separation factor and productivity of HOF-BTB[2], HIAM-103[3] and other kinds of adsorbents were calculated according to the data from corresponding references. Due to the unknown mass quality of the HOF-BTB sample used for breakthrough[2], we temporarily set it to be 1 g.

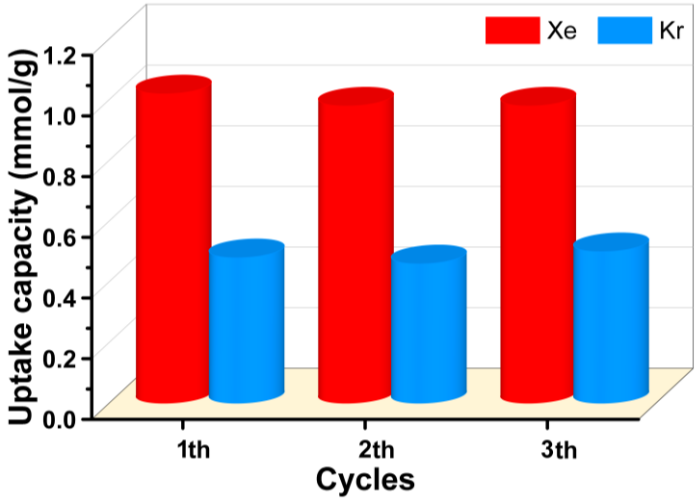

Figure S17. The dynamic uptake capacities of Xe (q_{Xe}) and Kr (q_{kr}) of HOF-FJU-8a in multiple breakthrough experiments.

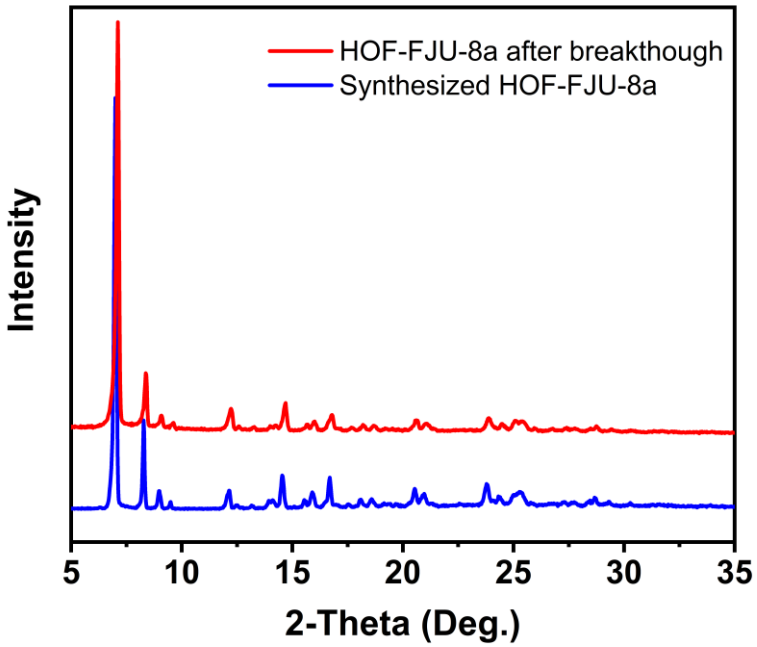

Figure S18. PXRD pattern of HOF-FJU-8a after breakthrough test.

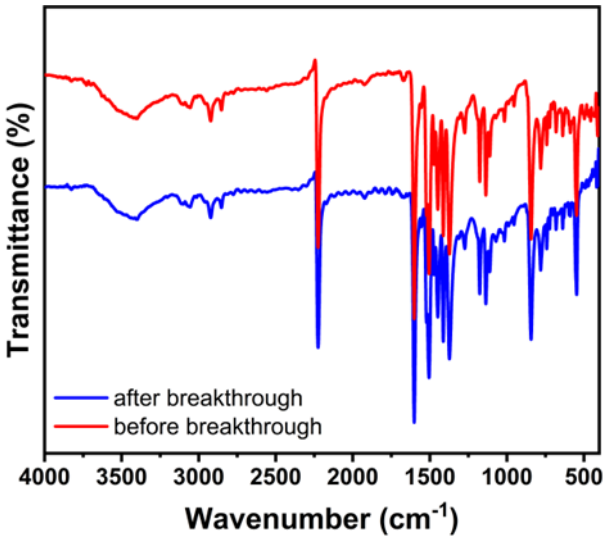

Figure S19. FTIR spectra of HOF-FJU-8a before and after dynamic breakthrough tests.

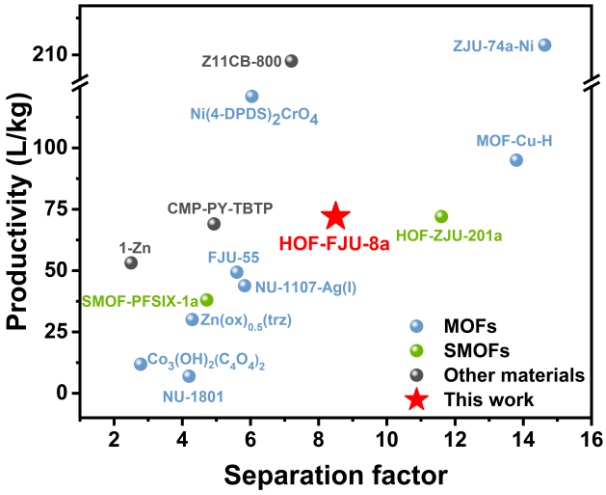

Figure S20. Comparison of the separation factor and Kr productivity of HOF-FJU-8a with other reported absorbents. 1-Zn: metal-organic polyhedral; Z11CB-800: activated carbon; CMP-PY-TBT: porous organic polymers.

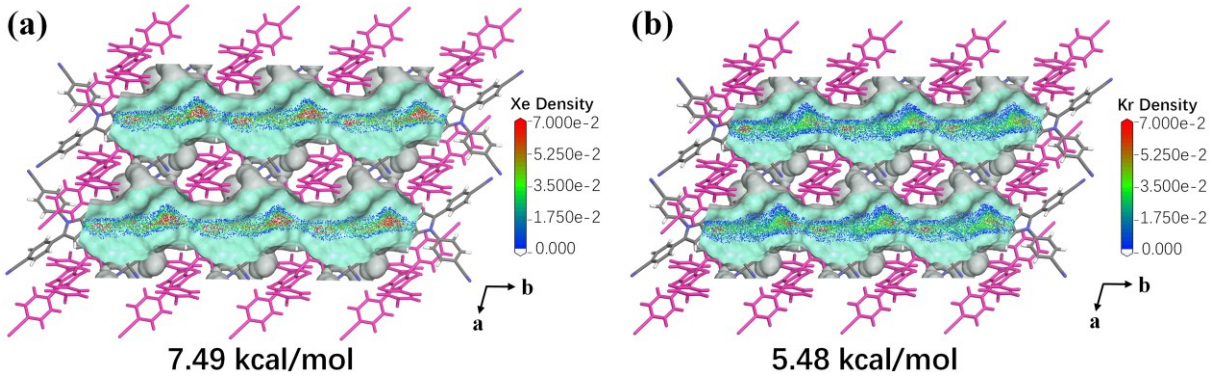

Figure S21. Density distribution of Xe (a) and Kr (b) in HOF-FJU-8a based on GCMC simulation.

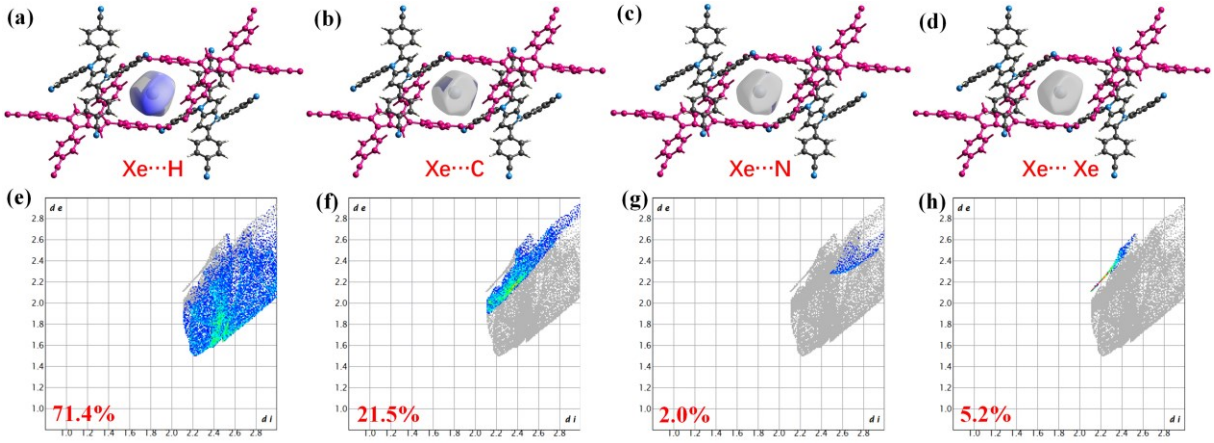

Figure S22. Hirshfeld surfaces analysis for the Xe-loaded HOF-FJU-8a.

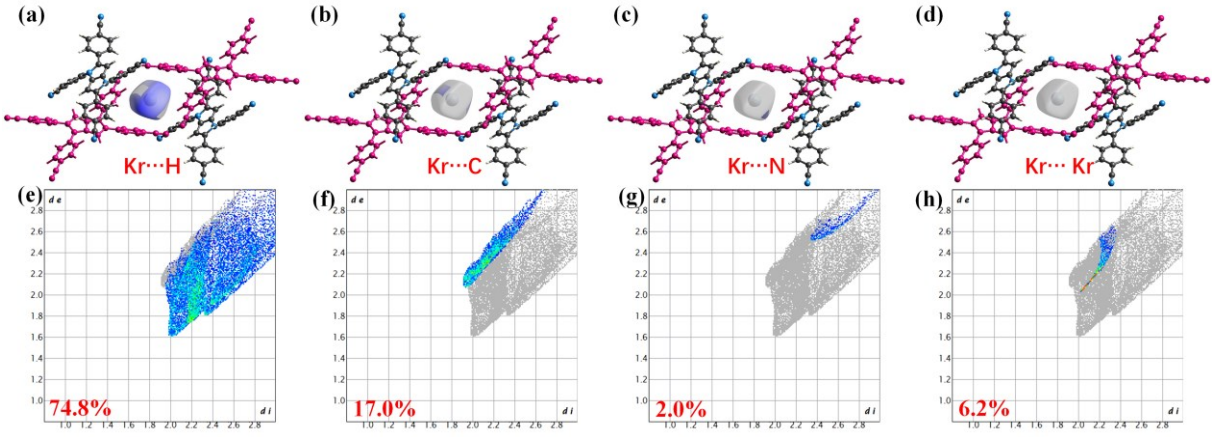

Figure S23. Hirshfeld surface analysis for the Kr-loaded HOF-FJU-8a.

Table S1. Crystal data and structure refinement.

Compounds	HOF-FJU-8a	HOF-FJU-8a·Xe	HOF-FJU-8a · Kr
CCDC	2286715	2286716	2286717
Empirical formula	$C_{34}H_{18}N_6$	$C_{34}H_{18}N_6$·Xe	$C_{34}H_{18}N_6$·$Kr_{0.56}$
Formula weight	510.54	641.84	557.05
Temperature/K	149.98(10)	149.99(10)	149.99(10)
Crystal system	triclinic	triclinic	triclinic
Space group	*P-1*	*P-1*	*P-1*
a/Å	10.9911(4)	10.9650(3)	10.9710(3)
b/Å	11.2098(4)	11.2030(3)	11.2013(3)
c/Å	13.1761(4)	13.1310(4)	13.1674(4)
α/°	105.237(3)	105.413(3)	105.253(3)
β/°	98.688(3)	98.431(3)	98.699(3)
γ/°	102.161(3)	102.074(2)	102.044(3)
Volume/Å^3	1494.07(9)	1485.22(8)	1489.89(8)
Z	2	2	2
ρ_{calc}g/cm^3	1.135	1.435	1.242
μ/mm^{-1}	0.550	9.333	1.535
F(000)	528.0	636.0	568.0
Crystal size/mm^3	0.28 × 0.06 × 0.03	0.28 × 0.06 × 0.03	0.28 × 0.06 × 0.03
Radiation	Cu Kα (λ = 1.54184)	Cu Kα (λ = 1.54184)	Cu Kα (λ = 1.54184)
Goodness-of-fit on F^2	1.056	1.071	1.086
Final R indexes [I>=2σ (I)]	R_1 = 0.0731, wR_2 = 0.2183	R_1 = 0.1302, wR_2 = 0.3388	R_1 = 0.0814, wR_2 = 0.2420
Final R indexes [all data]	R_1 = 0.0890, wR_2 = 0.2338	R_1 = 0.1474, wR_2 = 0.3507	R_1 = 0.0967, wR_2 = 0.2573
Largest diff. peak/hole / e Å^{-3}	0.67/-0.36	1.59/-1.46	0.83/-0.50

Table S2. Comparison of Xe capture properties in this work with some reported materials.

Compounds name	Surface area[a] (m^2 g^{-1})	Uptake (mmol g^{-1}) (RT and 1 bar) Xe	Kr	IAST[b] Selectivity	Q_{st} (kJ mol^{-1}) Xe	Kr	ΔQ (kJ mol^{-1})	Material type	Ref
ZJU-74a-Ni	694	3.29	1.39	74.1	41.7	21.8	19.9	MOF	4
$Co_3(OH)_2(C_4O_4)_2$	95	1.35	0.79	69.7	43.6	35.9	7.7	MOF	5
Ni(4-DPDS)$_2$CrO$_4$	317	1.61	1.0	23.7	28.5	15.4	13.1	MOF	6
MOF-Cu-H	868	3.19	1.61	16.7	33.4	25.5	7.9	MOF	7
ATC-Cu	600	5.0	2.7	13.9	NA	NA	NA	MOF	8
NU-1107-Ag(I)	1260	2.6[d]	0.83[d]	13.4	34.6	23.4	11.2	MOF	9
LPC-MOF	148	1.3	0.5	12.5[c]	28	22	6	MOF	10
Ag-MOF-303	716	3.35	1.12	10.4	28.2	18	10.2	MOF	11
$Zn(ox)_{0.5}(trz)$	546	2.72	1.29	10.2	29.0	14.0	15	MOF	12
FJU-55	377	1.41	0.62	10	39.4	14.4	25	MOF	13
NU-200	1260	4.9	1.28	9.3	28	20.6	7.4	MOF	14
NU-1801	1070	2.79	0.69	8.9	24.9	19.7	5.2	MOF	15
MOF-801	677	1.9	0.65	8.3	25.3	18.1	7.2	MOF	16
NKMOF-1-Ni	382	2.16	1.20	5.2	34.2	33.1	1.1	MOF	17
NU-403	NA	1.70	0.74	2.84	22.0	NA	NA	MOF	18
HOF-ZJU-201a	423	3.01	1.58	21.0	21.9	20.2	1.7	SMOF	19
SMOF-PFSIX-1a	389	2.29	1.08	6.9	38.4	10.5	27.9	SMOF	20
1-Zn	704	2.16	1.08	9.2	27	22	5	MOP	21
Z11CB-800	692	3.96	1.67	11.9	33.3	22.0	11.3	AC	22
IISERP-POF8	813	1.72	0.54	6.3	26	19	7	POP	23
PAF-45S	455	1.85	0.54	16.7[c]	31.0	19.3	11.7	POP	24
CMP-PY-TBTP	488	1.69	0.45[d]	11.9	28[d]	23[d]	5	POP	25
COP-4	2015	1.22	0.43	4.5	24.3	18.4	5.9	COF	26
ATFG-COF	244	1.72	0.54	6.3	25	16	9	COF	27

TFP-TAPA-Bu	487	3.82	1.27	9.7 [d]	NA	NA	NA	COF	28
Noria-BOC	NA	0.75	0.41	3.8	NA	NA	NA	POC	29
Noria	NA	1.55	0.64	9.4	26.9	21.4	5.5	POC	30
CC3	624	2.4	0.95	12.5	31.3	23.1	8.2	POC	31
HOF-BTB	955	2.01	0.416	6.1	18.7	14.3	4.4	HOF	2
HOF-40	234	1.56	0.44	11.2	32.8	24.4	8.4	HOF	32
HIAM-103	579	1.39	0.50	8.3	24.5	9.7	14.8	HOF	3
HOF-FJU-8a	375	1.81	0.77	12.1	30.6	15.6	15	HOF	**This work**

[a]BET Surface area; [b]From IAST calculation (Xe/Kr 20/80) at RT and 100 kPa; [c]From Henry's constant; [d]read from the figure from corresponding reference.

NA = Not available; MOF = Metal-organic framework; SMOF = Supramolecular MOFs; MOP = Metal-organic polyhedral; AC = Active carbon; POP = Porous organic polymer; COF = Covalent organic framework; POC = Porous organic cage; HOF = Hydrogen-bonded organic framework.

References

1. A. L. Myers and J. M. Prausnitz, *AIChE J.*, 1965, **11**, 121-127.
2. W.-G. Lee, T.-U. Yoon, Y.-S. Bae, K. S. Kim and S. B. Baek, *RSC Adv.*, 2019, **9**, 36808-36814.
3. F.-A. Guo, K. Zhou, J. Liu, H. Wang and J. Li, *Precis. Chem.*, 2023, DOI: 10.1021/prechem.1023c00040.
4. J. Pei, X.-W. Gu, C.-C. Liang, B. Chen, B. Li and G. Qian, *J. Am. Chem. Soc.*, 2022, **144**, 3200-3209.
5. L. Li, L. Guo, Z. Zhang, Q. Yang, Y. Yang, Z. Bao, Q. Ren and J. Li, *J. Am. Chem. Soc.*, 2019, **141**, 9358-9364.
6. F. Zheng, L. Guo, R. Chen, L. Chen, Z. Zhang, Q. Yang, Y. Yang, B. Su, Q. Ren and Z. Bao, *Angew. Chem. Int. Ed.*, 2022, **61**, e202116686.
7. S. Xiong, Y. Gong, S. Hu, X. Wu, W. Li, Y. He, B. Chen and X. Wang, *J. Mater. Chem. A*, 2018, **6**, 4752-4758.
8. Z. Niu, Z. Fan, T. Pham, G. Verma, K. A. Forrest, B. Space, P. K. Thallapally, A. M. Al-Enizi and S. Ma, *Angew. Chem. Int. Ed.*, 2022, **61**, e202117807.
9. W. Gong, Y. Xie, X. Wang, K. O. Kirlikovali, K. B. Idrees, F. Sha, H. Xie, Y. Liu, B. Chen, Y. Cui and O. K. Farha, *J. Am. Chem. Soc.*, 2023, **145**, 2679-2689.
10. X. Wang, F. Ma, S. Xiong, Z. Bai, Y. Zhang, G. Li, J. Chen, M. Yuan, Y. Wang, X. Dai, Z. Chai and S. Wang, *ACS Appl. Mater. Interfaces*, 2022, **14**, 22233-22241.
11. H. Wang, Z. Shi, J. Yang, T. Sun, B. Rungtaweevoranit, H. Lyu, Y.-B. Zhang and O. M. Yaghi, *Angew. Chem. Int. Ed.*, 2021, **60**, 3417-3421.
12. L. Yu, S. Xiong, Y. Lin, L. Li, J. Peng, W. Liu, X. Huang, H. Wang and J. Li, *Inorg. Chem.*, 2019, **58**, 15025-15028.
13. L. Gong, Y. Liu, J. Ren, A. M. Al-Enizi, A. Nafady, Y. Ye, Z. Bao and S. Ma, *Nano Res.*, 2022, **15**, 7559-7564.
14. W. Gong, Y. Xie, T. D. Pham, S. Shetty, F. A. Son, K. B. Idrees, Z. Chen, H. Xie, Y. Liu, R. Q. Snurr, B. Chen, B. Alameddine, Y. Cui and O. K. Farha, *J. Am. Chem. Soc.*, 2022, **144**, 3737-3745.
15. X. Song, Q. Huang, J. Liu, H. Xie, K. B. Idrees, S. Hou, L. Yu, X. Wang, F. Liu, Z. Qiao, H. Wang, Y. Chen, Z. Li and O. K. Farha, *ACS Appl. Mater. Interfaces*, 2023, **15**, 18229-18235.
16. Z. Yan, Y. Gong, B. Chen, X. Wu, Q. liu, L. Cui, S. Xiong and S. Peng, *Sep. Purif. Technol.*, 2020, **239**, 116514.
17. T. Wang, Y.-L. Peng, E. Lin, Z. Niu, P. Li, S. Ma, P. Zhao, Y. Chen, P. Cheng and Z. Zhang, *Inorg. Chem.*, 2020, **59**, 4868-4873.
18. K. B. Idrees, Z. Chen, X. Zhang, M. R. Mian, R. J. Drout, T. Islamoglu and O. K. Farha, *Chem. Mater.*, 2020, **32**, 3776-3782.
19. Y. Liu, H. Wu, L. Guo, W. Zhou, Z. Zhang, Q. Yang, Y. Yang, Q. Ren and Z. Bao, *Angew. Chem. Int. Ed.*, 2022, **61**, e202117609.
20. Y. Liu, J. Dai, L. Guo, Z. Zhang, Y. Yang, Q. Yang, Q. Ren and Z. Bao, *CCS Chem.*, 2022, **4**, 381-388.
21. W.-L. Shan, M.-L. Xu, H.-H. Hou, P. Zhao, Q.-Y. Zhang, M.-J. Yin and F. Luo, *Nano Res.*, 2023, **16**, 2536-2542.
22. Y. Gong, Y. Tang, Z. Mao, X. Wu, Q. Liu, S. Hu, S. Xiong and X. Wang, *J. Mater. Chem. A*, 2018, **6**, 13696-13704.
23. D. Chakraborty, S. Nandi, M. A. Sinnwell, J. Liu, R. Kushwaha, P. K. Thallapally and R. Vaidhyanathan, *ACS Appl. Mater. Interfaces*, 2019, **11**, 13279-13284.
24. J. Li, L. Huang, X. Zou, A. Zheng, H. Li, H. Rong and G. Zhu, *J. Mater. Chem. A*, 2018, **6**, 11163-11168.
25. Z. Yan, Y. Luo, B. Chen, F. Wang, L. Chen, Z. Wang, P. Zhao, J. Kang, Z. Fu, Y. Jin, Y. Wang and C. Xia,

Chem. Eng. J., 2023, **453**, 139934.

26. Q. Wang, S. Xiong, Z. Xiang, S. Peng, X. Wang and D. Cao, *Sci. China Chem.*, 2016, **59**, 643-650.
27. M. Yuan, X. Wang, L. Chen, M. Zhang, L. He, F. Ma, W. Liu and S. Wang, *Chem. Res. Chin. Univ.*, 2021, **37**, 679-685.
28. Z. Jia, Z. Yan, J. Zhang, Y. Zou, Y. Qi, X. Li, Y. Li, X. Guo, C. Yang and L. Ma, *ACS Appl. Mater. Interfaces*, 2021, **13**, 1127-1134.
29. M. Miklitz, S. Jiang, R. Clowes, M. E. Briggs, A. I. Cooper and K. E. Jelfs, *J. Phys. Chem. C*, 2017, **121**, 15211-15222.
30. R. S. Patil, D. Banerjee, C. M. Simon, J. L. Atwood and P. K. Thallapally, *Chem. Eur. J.*, 2016, **22**, 12618-12623.
31. L. Chen, P. S. Reiss, S. Y. Chong, D. Holden, K. E. Jelfs, T. Hasell, M. A. Little, A. Kewley, M. E. Briggs, A. Stephenson, K. M. Thomas, J. A. Armstrong, J. Bell, J. Busto, R. Noel, J. Liu, D. M. Strachan, P. K. Thallapally and A. I. Cooper, *Nat. Mater.*, 2014, **13**, 954-960.
32. L. Gong, Y. Ye, Y. Liu, Y. Li, Z. Bao, S. Xiang, Z. Zhang and B. Chen, *ACS Appl. Mater. Interfaces*, 2022, **14**, 19623-19628.